Numerical Simulations of Active Stabilization of Laminar Boundary Layers

Ralph W. Metcalfe,* Christopher J. Rutland,† James H. Duncan,‡ and James J. Riley§
Flow Research Company, Kent, Washington

The use of active wall forcing to modify the evolution of laminar boundary-layer flows has potential applications in delaying the transition to turbulence and hence in drag reduction. Here, the interaction between the wall motion and the fluid is investigated in order to gain insight into the physics of the stabilization process and also to determine the possibilities for stabilization by a passive wall medium. Direct numerical simulations of the time-dependent Navier-Stokes equations in two dimensions were performed using spectral numerical methods. The results of these simulations are analyzed to determine the relationship between the wall and fluid motion necessary for stabilization and also the energy balance achieved during this process. We show that the stabilization procedure used results in a net transfer of energy back into the mean flow and requires that the wall do work on the fluid. This holds true for highly inflectional mean velocity profiles as well as the Blasius profile. These energy fluxes differ significantly from those associated with flow stabilization by a compliant membrane.

Nomenclature

A_0 = amplitude of wall forcing
c = complex wave speed
DE = rate of change of perturbation energy
E_{DIS} = energy dissipation term
E_{PW} = pressure work term
E_{RS} = Reynolds stress production term
L_x = streamwise domain size
p = pressure
q^2 = $u^2 + w^2$
R = Reynolds number
R_{δ^*} = Reynolds number based on displacement thickness
T_n = Chebyshev polynomial of degree n
t = time
$\overline{U}$ = mean streamwise velocity
$\boldsymbol{u}$ = (u, w)
$\hat{\boldsymbol{u}}$ = Fourier transform of $\boldsymbol{u}$
u, w = velocity components
u', w' = perturbation velocity components
w_w = prescribed fluid velocity at the wall
x, z = streamwise, transverse coordinates
α = horizontal wavenumber
β = transverse mapping parameter
δ^* = displacement thickness
ϵ = dissipation
ϵ_f = fluctuating velocity dissipation
ϵ_M = mean velocity dissipation
η = wall displacement
θ = angle between wall and generated wave
λ = wavelength of unstable mode
ν = kinematic viscosity
π = pressure head
ρ = density
σ_{ij} = stress tensor
Φ = eigenfunction solution of Orr-Sommerfeld equation
ϕ = angle between w' at wall and w' at $z = z_0$
ω = vorticity

Presented as Paper 85-0567 at the AIAA Shear Flow Control Conference, Boulder, CO, March 12-14, 1985; received July 2, 1985; revision received Feb. 4, 1986.

*Senior Research Scientist. Member AIAA.
†Research Scientist (presently with Department of Mechanical Engineering, Stanford University, Stanford, CA).
‡Senior Research Scientist.
§Consultant; Professor, Department of Mechanical Engineering, University of Washington, Seattle. Member AIAA.

Introduction

THE possibility of drag reduction has created significant interest in the stabilization of boundary-layer flows. Experiments by Kramer[1] indicated that use of an appropriate compliant material could reduce drag, although his results have not yet been definitively verified by other experimentalists. His work has, however, stimulated considerable research in this area. Comprehensive reviews are given by Bushnell et al.,[2] McMichael et al.,[3] and Hansen et al.[4] While it appears possible to produce a modest delay in transition by the use of appropriate compliant materials, there is not yet unequivocal evidence of drag reduction in turbulent flows.

More recently, there have been some experimental and numerical studies of the active excitation of boundary-layer flows by wall forcing.[5-9] These studies have demonstrated the potential feasibility of flow stabilization. In this paper, we examine the effect of wall forcing on unstable waves in a laminar boundary layer and analyze the energy fluxes and balances associated with this stabilization process.

Numerical Methods

The basic equations of motion considered are the time-dependent Navier-Stokes equations in two spatial dimensions for an incompressible fluid. In terms of primitive variables, these are

$$\frac{\partial \boldsymbol{u}}{\partial t} + \boldsymbol{u} \times \boldsymbol{\omega} = -\nabla \pi + \nu \nabla^2 \boldsymbol{u}$$

$$\nabla \cdot \boldsymbol{u} = 0 \tag{1}$$

where $\boldsymbol{u} = (u, w)$ is the velocity field evaluated at $\boldsymbol{x} = (x, z)$ and t. The pressure head and the vorticity are

$$\pi = p + \tfrac{1}{2}\boldsymbol{u} \cdot \boldsymbol{u}$$

$$\boldsymbol{\omega} = \nabla \times \boldsymbol{u} \tag{2}$$

respectively. To obtain accurate numerical solutions to these equations, we have employed spectral numerical methods.[10]

In the transverse direction, we have mapped the semi-infinite region $z \in [0, \infty]$ into the finite interval $\zeta \in [-1, +1]$ by the relation

$$\zeta = \frac{z-\beta}{z+\beta} \tag{3}$$

We have used $\beta = 1.1\delta^*$ to ensure adequate resolution in the boundary layer. Spectral simulations using mappings of the form in Eq. (3) have been shown to work very well.[11] In the streamwise direction, the dependent variables are expanded in Fourier series, whereas in the transverse direction a Chebyshev expansion is employed. Thus, velocity components are represented as

$$\boldsymbol{u}(x,\zeta,t) = \sum_{|k|<K} \sum_{n=0}^{N} \hat{\boldsymbol{u}}(k,n,t) \exp\left(\frac{2\pi i k x}{L_x}\right) T_n(\zeta) \tag{4}$$

These methods have been applied to a variety of flow simulation problems by Orszag et al.[12,13]; the code used in these simulations was developed in collaboration with Prof. Orszag.

Time differencing is performed using a second-order Adams-Bashforth scheme on the nonlinear terms and an implicit time-splitting method on the pressure and viscous terms.[13] Periodic boundary conditions are applied in the streamwise direction. Thus, these simulations correspond to a *temporally* rather than *spatially* growing boundary layer. At the wall, we have applied a linearized boundary condition for the wall motion, which is equivalent to an exact boundary condition for suction and blowing through the wall. Let $\boldsymbol{u} = (\bar{U} + \boldsymbol{u}', w')$ at the surface $z_w = \eta(x,t)$. Then, the condition is $u'(x,0,t) = 0$, $w'(x,0,t) = w(x,t)$. The linearization of this bottom boundary condition requires that all relevant flow quantities be evaluated at $z = 0$, rather than on the actual surface $z = \eta(x,t)$. This is valid as long as the amplitude of the wall motion remains small compared to its wavelength and, in the vicinity of the wall, the fluctuating velocity is small compared to the mean. Thus, the boundary condition is linearized if considered as wall motion, but exact (not linearized) if considered as blowing or suction. Numerically, the implementation of a linearized boundary condition results in a substantial simplification of the numerical code as well as an order of magnitude increase in the execution speed.

In these simulations, we have focused on the effects of wall motion on unstable Tollmien-Schlichting (TS) waves. Our initial conditions are defined using solutions of the Orr-Sommerfeld stability equation

$$(\bar{U}-c)(\Phi'' - \alpha^2\Phi) - \bar{U}''\Phi = \frac{i\nu}{\alpha R}(\Phi'''' - 2\alpha^2\Phi'' + \alpha^4\Phi) \tag{5}$$

In these simulations, $\bar{U}$ is a Blasius mean velocity profile. The perturbation velocity components of the TS wave can be written as

$$u(x,z,t) = \Phi'(z)\, e^{i\alpha(x-ct)}$$
$$w(x,z,t) = -i\alpha\Phi(z)\, e^{i\alpha(x-ct)} \tag{6}$$

Energy Balance

To gain some insight into the dynamics of the interaction between the wall motion and the fluid, it is helpful to analyze the kinetic energy balance. The appropriate equations can be derived, for example, from the energy equation for an incompressible, viscous fluid,[14]

$$\frac{1}{2}\frac{\partial q^2}{\partial t} + \frac{\partial}{\partial x}\left(\frac{q^2}{2}u + \frac{p}{\rho}u - u\sigma_{11} - w\sigma_{13}\right) + \frac{\partial}{\partial z}\left(\frac{q^2}{2}w + \frac{p}{\rho}w - u\sigma_{31} - w\sigma_{33}\right) = -\epsilon \tag{7}$$

where

$$\sigma_{ik} = \nu\left(\frac{\partial u_i}{\partial x_k} + \frac{\partial u_k}{\partial x_i}\right)$$
$$\epsilon = \frac{\nu}{2}\sum_{i,k}\left(\frac{\partial u_i}{\partial x_k} + \frac{\partial u_k}{\partial x_i}\right)^2 \tag{8}$$

Assuming the flowfield is periodic in x with period λ, Eq. (7) can be integrated to yield, in terms of the mean and fluctuating components,

$$\int_0^\infty \int_{x_0}^{x_0+\lambda} \frac{1}{2}\frac{\partial q'^2}{\partial t}\,dx\,dz + \lambda\int_0^\infty \frac{1}{2}\frac{\partial \bar{U}^2}{\partial t}\,dz - \int_{x_0}^{x_0+\lambda} \frac{pw}{\rho}\bigg|_{z=0} dx = -\int_0^\infty \int_{x_0}^{x_0+\lambda} \epsilon\,dx\,dz \tag{9}$$

Similarly, the energy balance for the mean motion can be derived from the following equation,[14] where the overbar (¯) represents averaging over one period in the x direction:

$$\frac{1}{2}\frac{\partial \bar{U}^2}{\partial t} + \frac{\partial}{\partial z}\left(\overline{u'w'}\bar{U} - \bar{U}\bar{\sigma}_{31}\right) = -\epsilon_M + \overline{u'w'}\frac{\partial \bar{U}}{\partial z} \tag{10}$$

where

$$\bar{\sigma}_{31} = \nu\frac{\partial \bar{U}}{\partial z}$$
$$\epsilon_M = \frac{\nu}{2}\sum_{i,k}\left(\frac{\partial \bar{U}_k}{\partial x_i} + \frac{\partial \bar{U}_i}{\partial x_k}\right)^2 = \nu\left(\frac{\partial \bar{U}}{\partial z}\right)^2 \tag{11}$$

Integrating over z and applying the following boundary conditions,

$$\bar{U} = \frac{\partial \bar{U}}{\partial x} = 0 \quad \text{at } z = 0$$
$$\left[\bar{U} \to \bar{U}_\infty, \text{ and } \frac{\partial \bar{U}}{\partial z},\ u', w' \to 0\right] \text{ as } z \to \infty \tag{12}$$

the mean energy equation can then be written

$$\int_0^\infty \frac{1}{2}\frac{\partial \bar{U}^2}{\partial t}\,dz = -\int_0^\infty \epsilon_M\,dz + \int_0^\infty \overline{u'w'}\frac{\partial \bar{U}}{\partial z}\,dz \tag{13}$$

Finally, the energy equation for the perturbation velocity field can be obtained by subtracting Eq. (13) from Eq. (9),

$$\int_0^\infty \int_{x_0}^{x_0+\lambda} \frac{1}{2}\frac{\partial q'^2}{\partial t}\,dx\,dz = \int_{x_0}^{x_0+\lambda} \frac{p'w'}{\rho}\bigg|_{z=0} dx - \int_0^\infty \int_{x_0}^{x_0+\lambda} u'w'\frac{\partial \bar{U}}{\partial z}\,dx\,dz - \int_0^\infty \int_{x_0}^{x_0+\lambda} \epsilon_f\,dx\,dz \tag{14}$$

where

$$\epsilon_f = \frac{\nu}{2}\sum_{i,k}\left(\frac{\partial u_k'}{\partial x_i} + \frac{\partial u_i'}{\partial x_k}\right)^2 \tag{15}$$

The term on the left-hand side of Eq. (14) is the rate of change of the perturbation energy DE; the first term on the right-hand side is the pressure work or pressure diffusion term E_{PW}; the second, E_{RS}, is the Reynolds stress production; and the last is the dissipation E_{DIS}.

Code Validation

To test the accuracy of the code, simulations of the evolution of an unstable TS wave in the absence of boundary forcing were performed. The initial conditions were obtained

by solving the Orr-Sommerfeld equation (5). The Reynolds number was $R_{\delta *} = 1000$ at a wavenumber $\alpha\delta^* = 0.225$, which is approximately the wavenumber of the most unstable linear mode. The initial amplitude was taken to be $w'_{\max}/\bar{U}_\infty \simeq 1 \times 10^{-5}$, so that nonlinear effects were small. In the streamwise direction, the computational domain was taken to be the wavelength of the unstable mode and the time step $\Delta t = 0.03$. Eight Fourier modes were used in the x direction and 33 Chebyshev modes were used in the z direction. For this simulation, the computed growth rate was within about 1% of the theoretical estimate and the phase speed of the TS wave, which should be $0.35\ \bar{U}_\infty$, was also in agreement with this value to within this accuracy. The energy balance for the mean flow [Eq. (13)] was also checked, and the two dominant terms, the loss of energy by the mean flow and the dissipation, were found to balance within 2%. In addition, this dissipation term can be estimated independently for a Blasius mean velocity profile,[15]

$$\int_0^\infty \epsilon_M \, dz = \int_0^\infty \frac{\nu}{2}\left(\frac{\partial \bar{U}}{\partial z}\right)^2 dz \simeq 0.224 \frac{\bar{U}_\infty^3}{R_{\delta *}} = 0.224 \times 10^{-3} \tag{16}$$

This compared well with the computed value of 0.2239×10^{-3}.

It is much more difficult to validate the accuracy of the code when wall forcing is present, since analytic solutions in this case are difficult to obtain. However, we have made comparisons for a model problem in which viscous effects are small due to the short times involved. In this case, potential flow is a good approximation. The wall forcing is introduced as a simple sinusoidal wave in the w' velocity component at $z = 0$. To minimize the generation of high-frequency transients, the wall velocity was defined by the relation

$$w'|_{z=0} = w_0(t)\cos k(x - ct) \tag{17}$$

where

$$w_0(t) = \frac{A_0}{2}\left[1 - \frac{\tan^{-1}(t_2 - t)}{\tan^{-1}(t_2 - t_0)}\right] \tag{18}$$

For the potential flow solution, we assume a uniform mean velocity, which implies that the Reynolds stress terms in Eq. (14) are all zero. Since the flow is also inviscid, Eq. (14) reduces to

$$\int_0^\infty \int_{x_0}^{x_0+\lambda} \frac{1}{2}\frac{\partial q'^2}{\partial t}\, dx\, dz = \int_{x_0}^{x_0+\lambda} \frac{p'w'}{\rho}\bigg|_{z=0} dx \tag{19}$$

Based on potential flow theory, the following expression for the pressure work term can be derived:

$$\frac{\overline{p'w'}}{p} = \frac{1}{2}\frac{dw_0}{dt}\frac{w_0}{k} \tag{20}$$

Figure 1 is a plot of this term, normalized by $A_0^2\bar{U}_\infty/\alpha\delta^*$, and the rate of change of the energy [Eq. (19)] from the numerical simulation. Time is normalized by $\bar{U}_\infty/\delta^*$. The other relevant parameters were $t_0 = 0$, $t_2 = 15$, $c/\bar{U}_\infty = 0.384$, $\alpha\delta^* = 0.225$, $\bar{U}_\infty = 1$, and $A_0 = 3.25 \times 10^{-7}$. The agreement is good, considering that the potential flow solution permits no residual transient fluid motion after the wall motion becomes constant at $t \simeq 22$. Such motion is evident in the computed solution. This is an important consistency check on the numerical results, since most of the simulations reported in this paper employ a similar wall-forcing algorithm.

Wall-Forcing Algorithm

The main objective of this work was to determine possible wall-forcing schemes that could stabilize TS waves. One possibility is to generate a wave that will "cancel out" the disturbance. McMurray et al.[6] have performed successful numerical simulations of such a process. This has also been done experimentally. For example, Milling[5] was able to cancel out artificially generated, uniform-frequency TS waves by setting up another TS wave generator downstream of the first and running it 180 deg out of phase with the first. Liepmann et al.[7,8] were able to stabilize TS waves by properly phased boundary-layer heating. More recently, Kuhn et al.[9] and Biringen[16] have also performed numerical simulations of flow stabilization by active wall forcing, with some success.

McMurray et al.[6] showed that sinusoidal wall forcing at the same wavelength as the TS wave and with the proper phase relationship could produce attenuation. However, since continued forcing would eventually generate a large out-of-phase disturbance, a "smart wall" algorithm was proposed in which the phase and amplitude of the wall forcing was linked to the phase and amplitude of the w' velocity component in the fluid at some distance from the wall. This algorithm was found to work well and not only on the TS wave; it also was able to stabilize more complex flow structures such as wave packets. In the next section, we will analyze the energy balance during this active wall forcing.

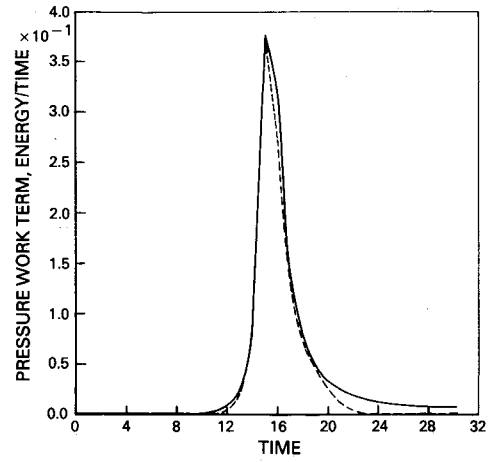

Fig. 1 Comparison of computed rate of energy change (solid line) and analytically predicted pressure work term (dashed line) with wall forcing for potential flow.

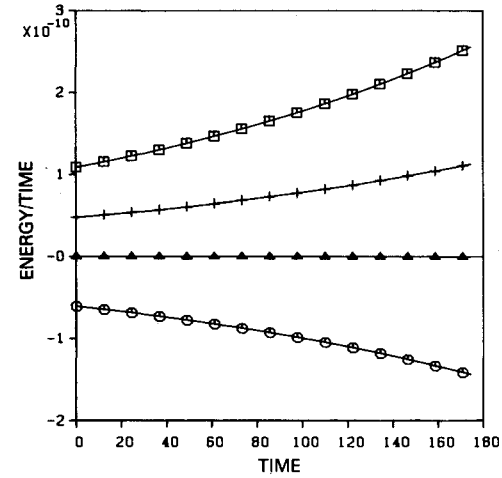

Fig. 2 Energy balance for an unstable TS wave (case C): + = DE, △ = E_{PW}, □ = E_{RS}, ○ = E_{DIS}. See Eq. (14).

Analysis of Energetics

Three basic simulations were performed: 1) smart wall forcing in the presence of an unstable TS wave (case A); 2) the same wall forcing without a TS wave (case B); and 3) the TS wave with no wall forcing (case C).

The energy balance for a freely propagating TS wave is shown in Fig. 2 (case C). This simulation was done at $R_{\delta^*} = 1000$ and $\alpha\delta^* = 0.225$, with time normalized by $\delta^*/\bar{U}_\infty$ and energy by $\bar{U}_\infty^2$. The Reynolds stress production term [E_{RS}, see Eq. (14)] is positive and growing in time, indicating a transfer of energy from the mean flow into the TS wave. The dissipation (E_{DIS}) is negative, as energy in the TS wave is viscously damped. The pressure work term is zero, since there is no wall motion. For this unstable wave, the transfer from the mean flow is greater than the dissipation so that there is a net growth of the perturbation energy (DE). Of course, the total kinetic energy of the flow decreases with time due to viscous dissipation. (Relevant and detailed discussions of energy balance for flow over a membrane are given by Landahl[17] and Benjamin.[18]) The perturbation velocity field corresponding to the TS wave is shown in Fig. 3 at $t = 17.4$.

The modified "smart wall" algorithm applied in these simulations was defined as follows. The wall motion was defined by the function

$$G(x,t) = B(t)\,w'(x+\phi, z_0, t) \tag{21}$$

where $\phi = 95$ deg and $z_0 = 2\delta^*$. This value of z_0 was chosen because it is the level at which w' of the TS wave for the Blasius mean velocity profile is a maximum. ϕ is the phase angle between w' at the wall and w' at z_0. Another important angle is θ, which is the phase angle between the wall and the wave generated by the wall. If $90 \le \phi + \theta \le 270$ deg and the wall-generated wave is similar to the TS wave, then some wave cancellation effect is expected. A number of test calculations showed that this was indeed the case. Conversely, if ϕ was chosen such that

$$270 < \phi + \theta < 90 \text{ deg} \tag{22}$$

the wall forcing could produce a significant enhancement in the growth of the TS wave. The value of $\phi = 95$ deg was determined to be optimal for stabilization after several test runs. The corresponding value of θ in this case was 85 deg. Thus, if the wall forcing begins to reduce the wave amplitude w' at $z = z_0$, then the amplitude of the wall forcing will also decrease.

The function $B(t)$ was defined the same as $w_0(t)$ in Eq. (18) to minimize the generation of transients. This is a smoothly varying "bridge" function in which the rate of initiation or termination of the wall forcing is a function of the parameter t_0. Test runs showed that minimal transients were generated with $\Delta t_r = |t_0 - t_2| = 10$. In case A, we used $\Delta t_r = 8.7$ with the wall being turned on at $t_2 = 8.7$ and off at $t_2 = 125$. The parameter A was 0.3, which corresponds to wall forcing in which the w velocity at the wall reaches 30% of the value at $z = z_0$.

The energy balance for case A is shown in Fig. 4. The simulation begins with the same unstable TS wave as in case C, so that the pressure work term is zero, the Reynolds stress production and perturbation energy growth positive, and the dissipation negative. The introduction of wall motion at $t \simeq 8$ causes the pressure work term to become positive, indicating that the wall is working on the fluid. Simultaneously, however, the Reynolds stress term becomes negative, so that the net energy change also becomes negative, i.e., the flow is being stabilized. Equivalently, since the total kinetic energy of the flow for a TS wave is decreasing with time (i.e., it is a class A wave[18]), adding energy with the pressure work term stabilizes the flow. At $t \simeq 125$, the wall is turned off and the flow again becomes unstable.

Part of the stabilizing effect is due to the generation of an out-of-phase wave that, superposed on the TS wave, reduces its amplitude. However, the behavior of the Reynolds stress term suggests that there is another stabilizing mechanism. Figure 5 shows the behavior of this term in the case of two identical TS waves as a function of the phase angle between

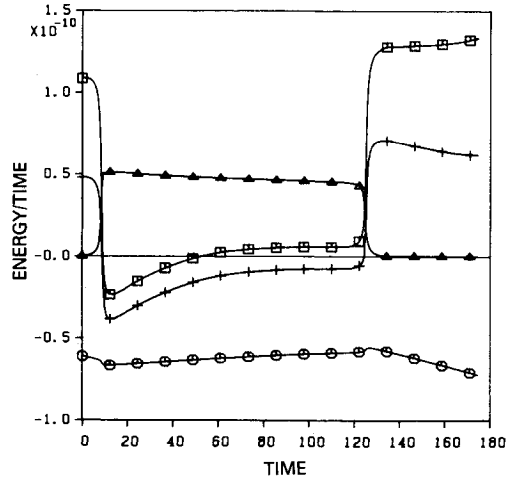

Fig. 4 Energy balance for "smart wall" forcing of TS wave (case A): + = DE, △ = E_{PW}, □ = E_{RS}, ○ = E_{DIS}.

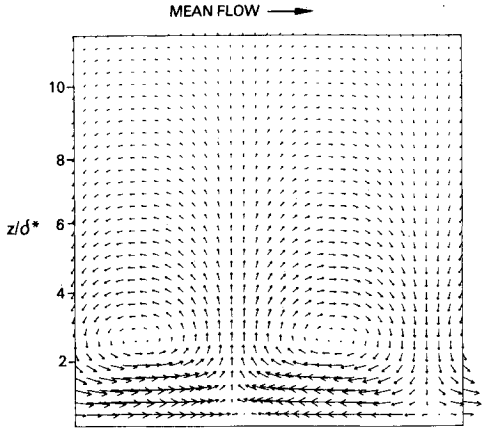

Fig. 3 Perturbation velocity field for TS wave at $t = 17.4$ ($R_{\delta^*} = 1000$, $\alpha\delta^* = 0.225$).

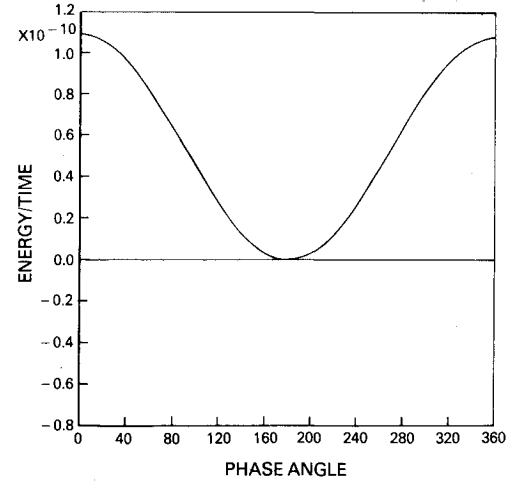

Fig. 5 Reynolds stress production as a function of phase angle between two identical TS waves.

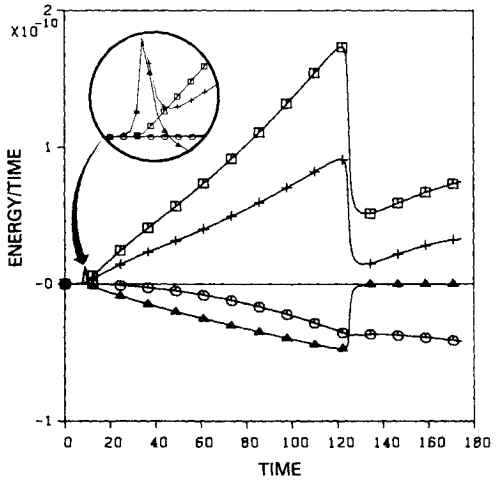

Fig. 6 Energy balance with wall forcing alone (case B): $+ = DE$, $\Delta = E_{PW}$, $\square = E_{RS}$, $\bigcirc = E_{DIS}$.

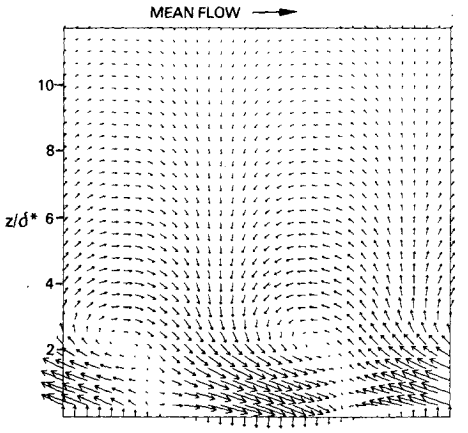

Fig. 7 Perturbation velocity field for wall-forced wave (case B) at $t = 17.4$.

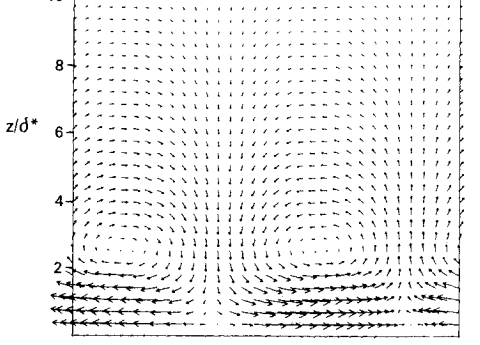

Fig. 8 Perturbation velocity field for wall-forced wave (case B) at $t = 105$.

them. Note that the minimum value of the Reynolds stress term is zero when the two waves are exactly out of phase. Thus, a pure wave cancellation effect could not account for the negative Reynolds stress.

An examination of the structure of the wall-generated wave can shed some light on this issue. Case B was a simulation performed with identical wall motion to that in case A, but without the freely propagating TS wave present. This was accomplished by running simulation A first and recording the exact wall motion, which was then used in case B. Figure 6 is a plot of the energy balance terms for case B. This shows that, after an initial transient period, a rapidly growing, unstable wave is produced, which continues to grow, although at a slower rate, after the wall forcing is terminated at $t \simeq 125$. Figure 7 is a plot of the perturbation velocity field of this wall-forced wave at $t = 17.4$, shortly after the wall motion is initiated. A comparison with the structure of the freely propagating TS wave (Fig. 3) shows that the case B wave, unlike case C, is no longer symmetric about vertical lines passing through nodes where $u' = 0$. This transient distortion is due to the interaction of the symmetrically generated wall disturbance with the mean flow. What is of particular interest is that this low-amplitude transient wave, when generated at the proper phase angle to the original TS wave, can create a negative Reynolds stress and thus stabilize the flow more effectively than by simple wave cancellation.

Shortly after the wall motion is initiated, a strong potential effect is produced. This can be seen in the blown up portion of the plot shown in Fig. 6, which shows the evolution of the energy balance terms for case B at early times. The pressure work term at first behaves much like it did in our earlier test problem [Eq. (20), Fig. 1]. It is initially positive, indicating that work is being done on the fluid. As the mean flow begins to act on the disturbance, however, the Reynolds stress production quickly builds up and the sign of the work term is reversed as the phase of the wave shifts relative to that of the wall. Eventually, as the amplitude of the wall forcing diminishes at later times, the structure of the forced wave becomes symmetric like that of the TS wave. This can be seen by comparing Figs. 8 and 3. Note that at these later times, the Reynolds stress production term in the forced wall run (case A) approaches zero. This suggests that, unlike earlier times, the stabilization mechanism at this point is almost entirely one of cancellation due to the superposition of nearly identical, out-of-phase waves.

As previously discussed, when the wall motion is in phase with the TS wave [i.e., Eq. (22) is satisfied], the growth rate of the TS wave is enhanced. Consequently, the behavior of the energy balance terms is also quite different than in the out-of-phase forcing case (Fig. 4). Qualitatively, the behavior is like that for case B between $t = 20$ and 100 (cf, Fig. 6). The pressure work term is negative, as is the dissipation, but this is counterbalanced by a significant enhancement in the Reynolds stress production, so that the net rate of perturbation energy production is larger. The greatest increase in growth rate occurs at about $\phi = 275$ deg, i.e., about 180 deg from the optimal choice of ϕ for the "smart wall" runs.

An examination of the vertical structure of the energy balance terms provides some useful information about the dynamics of the energy interchange between the wall and the fluid. Figure 9 is a plot of the Reynolds stress production as a function of distance from the wall for cases A, B, and C at $t = 30$. For the freely propagating TS wave (case C), the Reynolds stress production peaks near the critical level for the TS wave, which is at $\eta/\delta^* \sim 0.62$. While the mean shear is nearly uniform below the critical layer, it decreases sharply above this level. For case B, the Reynolds stress production is similar, but much lower in amplitude. However, when the two modes are combined out of phase (case A), this term becomes negative over a significant portion of the domain, so that the net production is negative. Thus, a small perturbation of the right type to an unstable TS wave can completely disrupt the Reynolds stress production mechanism. The phase of the wave in case B is, of course, critical to the net effect on the Reynolds stresses. The addition of the waves in cases B and C with phase 180 deg different from that in case A would result in an increased Reynolds stress production.

Figure 10 is a similar plot of the pressure work term for the three cases. For the freely propagating TS wave (case C), this term integrates to zero over the entire domain (Fig. 2). None-

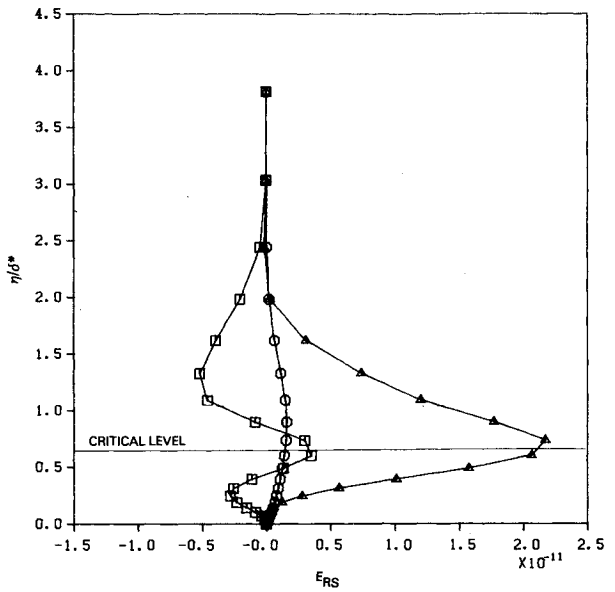

Fig. 9 Reynolds stress production (E_{RS}) as a function of distance from the wall at $t = 30$: □ = case A, ○ = case B, △ = case C.

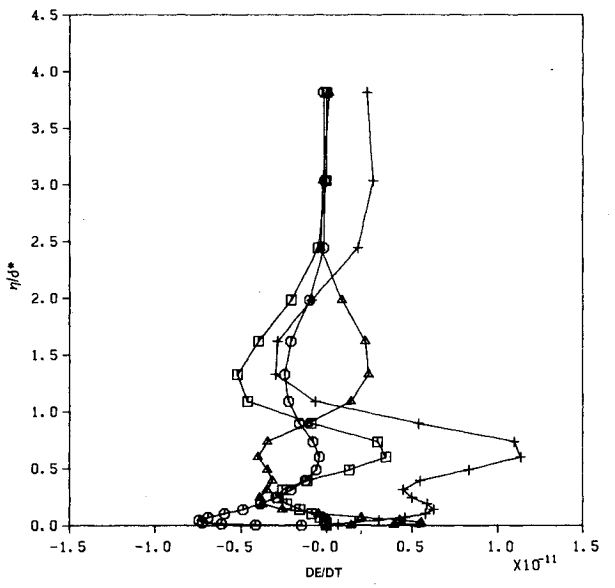

Fig. 11 Energy balance terms as functions of distance from the wall at $t = 30$: □ = case A, ○ = case B, △ = case C.

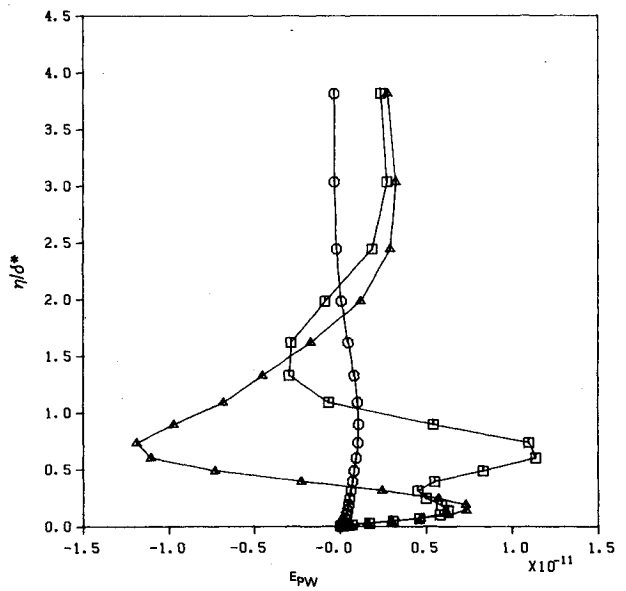

Fig. 10 Pressure work term (E_{PW}) as a function of distance from the wall at $t = 30$: □ = case A, ○ = case B, △ = case C.

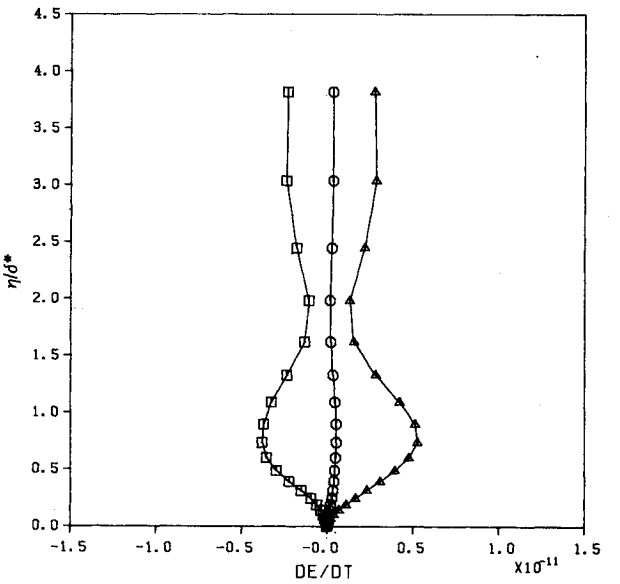

Fig. 12 Rate of change of perturbation energy (DE) as a function of distance from the wall at $t = 30$: □ = case A, ○ = case B, △ = case C.

theless, it plays a very important role in the energy dynamics. In this case, it is really a pressure diffusion term, which serves to transfer the energy from the region of maximum Reynolds stress production near the critical layer to a layer near the wall where dissipation is high and also to a region near the top of the boundary layer where it serves to enhance the growth of the layer. In case B, the structure is quite different, since it now represents mainly a transfer of energy from the fluid to the wall. Again, as with the Reynolds stress production term, the superposition of these two modes results in a strong nonlinear effect (case A). The pressure work term is now positive as the wall does work on the fluid to stabilize the TS wave.

Four terms are plotted in Fig. 11 for case A so that their relative magnitudes can be compared. For clarity, we have rewritten the dissipation term [Eq. (15)] as

$$E_{DIS} = E_{VS} + E_{VDIS} \tag{23}$$

where

$$E_{VS} = \nu \frac{\partial}{\partial x_i} \overline{u_k \left(\frac{\partial u_i}{\partial x_k} + \frac{\partial u_k}{\partial x_i} \right)} \tag{24}$$

and

$$E_{VDIS} = -\nu \overline{\left(\frac{\partial u_k}{\partial x_i} + \frac{\partial u_i}{\partial x_k} \right) \frac{\partial u_k}{\partial x_i}} \tag{25}$$

E_{VS}, the viscous stress work or viscous diffusion term, serves to diffuse energy away from the critical level production region, as does the pressure work term in case C. This term integrates to zero over the entire domain, so there is no net contribution to the energy balance. E_{VDIS}, the viscous dissipation term, removes mechanical energy from the fluid, with its maximum effect near the wall. It is interesting that the viscous dissipation is nearly zero at the critical level, where Reynolds

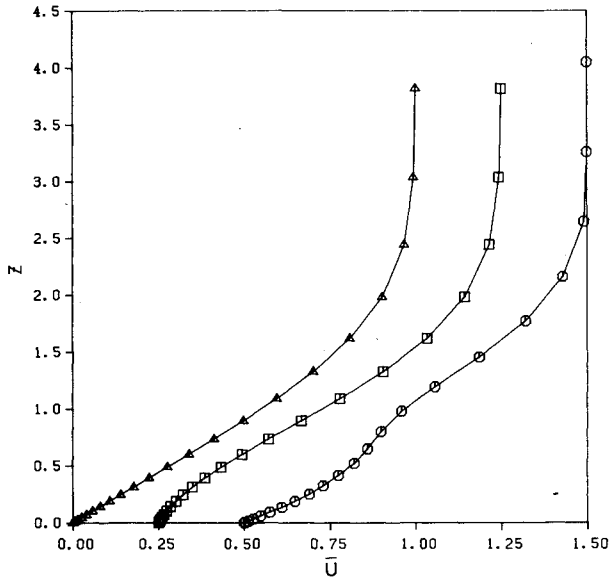

Fig. 13 Comparison of inflectional profiles: □ = Gad-el-Hak et al.[19] (critical $R_{\delta^*} \simeq 165$), ○ = Klebanoff et al.[20] (critical $R_{\delta^*} \simeq 50$), △ = Blasius case (critical $R_{\delta^*} \simeq 515$).

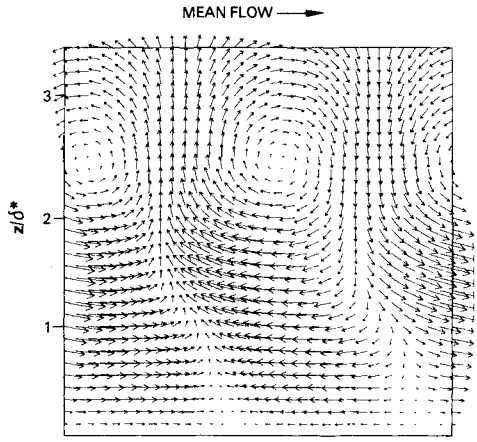

Fig. 14 Perturbation velocity field for most unstable mode with Klebanoff mean velocity profile at $t = 29$ ($R_{\delta^*} = 200$).

stress production is at a maximum. These two terms, unlike the Reynolds stress production and pressure work, are almost unaffected by the wall motion and the plots are virtually identical for case C.

The net effect on the energy balance is shown in Fig. 12. For the freely propagating TS wave, there is a net positive growth in the perturbation energy throughout the domain, with peak growth occurring near the critical level where the perturbation energy is at a maximum. This is also true in case B. During stabilization by wall forcing (case A), the energy decays in a manner similar to its growth in case C. Thus, the stabilization process does not significantly modify the vertical structure of the TS wave.

Inflectional Profiles

The simulations discussed in the previous section dealt with TS waves in a Blasius boundary layer. We have also examined the interaction between wall-forced waves and unstable modes when the mean velocity profile is inflectional. In this situation, inviscid instabilities that have much larger growth rates than those for the Blasius case can exist. Such instabilities are more representative of flow evolution during the transition to turbulence. The simulations described in this section are two-dimensional and therefore do not include relevant three-dimensional effects. Nonetheless, it is of interest to examine

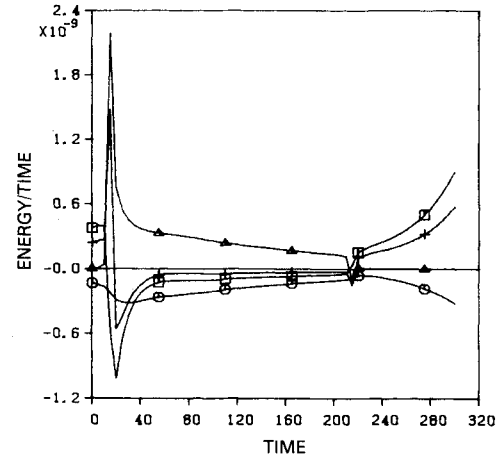

Fig. 15 Energy balance for "smart wall" forcing of most unstable mode with Klebanoff mean velocity profile: + = DE, △ = E_{PW}, □ = E_{RS}, ○ = E_{DIS}.

the differences in the response of the viscously and inviscidly unstable modes.

Our first simulation involved an inflectional profile taken from a study by Gad-el-Hak et al.[19] of laminar flow over a decelerating plate (Fig. 13). For this profile (taken at $t = 5$ in Fig. 9 of that paper), the critical Reynolds number was $R_{\delta^*} \simeq 165$. At the Reynolds number used in these simulations, $R_{\delta^*} = 1000$, the growth rate of the most unstable mode was much larger than for the Blasius case for the same Reynolds number. Here $c_i = 0.059$ [cf, Eq. (6)] at $\alpha\delta^* = 0.41$, compared with $c_i = 0.011$ for the TS wave in a Blasius boundary layer. After performing a number of simulations, it was determined that stabilization of this mode was possible. However, a larger amplitude of forcing was necessary, with $A = 0.6$ rather than 0.3 for the Blasius case. Also, the phase shift for optimum stabilization of the wall-generated wave differed from the Blasius case, being approximately $\phi = 125$ deg rather than 95 deg [cf, Eq. (21)]. The corresponding value of θ was 55 deg.

A more highly inflectional profile was also examined (Fig. 13). Fig. 23 from Klebanoff et al.[20] shows a mean velocity profile in a boundary layer near the transition point. The critical Reynolds number for this profile is about 50, compared with 165 and 515 for the Gad-el-Hak and Blasius profiles, respectively. At $R_{\delta^*} = 1000$, the most unstable mode had $c_i = 0.094$, a much larger growth rate than the Gad-el-Hak profile. Although a complete stabilization of this mode was not obtained at this high Reynolds number, significant reduction in growth rate was obtained using $A = 1.0$ and $\phi = 0$ deg.

Several simulations were also performed at a lower Reynolds number, $R_{\delta^*} = 200$. Due to the presence of two inflection points in the mean velocity profile, the structure of the most unstable mode is more complex than for the Blasius profile (compare Figs. 3 and 14). In addition, the structure of the wall-generated wave is also more complex, so that stabilization based on simple wave cancellation is not obvious. In this case, $\theta = 75$ deg, so that $\phi + \theta = 140$ deg, not 180 deg as in the previous cases. Even at this Reynolds number, the growth rate of this disturbance was $c_i = 0.058$ for $\alpha\delta^* = 0.36$. Nonetheless, with $A = 1$ and $\phi = 65$ deg, stabilization of the wave was achieved. The energy balance plot is shown in Fig. 15. The behavior of the important terms is qualitatively the same as for the Blasius profile (Fig. 4).

Discussion

The flow stabilization process described in this paper is associated with a dramatic change in the behavior of the Reynolds stress production term. Application of wall forcing of the proper phase causes the Reynolds stress term to become negative, indicating a feed of energy from the perturbed flow back into the mean. This shows that a relatively low-amplitude perturbation of an unstable wave can effectively

stabilize that wave. However, this perturbation wave generated by the wall is itself highly unstable, so that the amplitude of the wall forcing must be constrained.

The phase angle of the wall motion relative to the fluid wave during stabilization is such that the crest of the wave at the wall lags the high-pressure region in the fluid. This is consistent with the wall doing work on the fluid and explains the positive pressure work term. Although the wall is putting energy into the fluid, the larger effect of disrupting the Reynolds stress production mechanism is created, so that the net result is a decay in the perturbation energy consistent with the behavior of a class A wave.[17,18] We have performed a number of simulations in which the phase, phase speed, and amplitude of the wall forcing were varied. Under those conditions in which stabilization was achieved, the energetics analysis is qualitatively the same as just described. The necessity for the wall to do work on the fluid in this stabilization process makes it difficult to hypothesize how a purely passive wall material, such as a compliant coating, could emulate this wall motion.

In recent numerical simulations, Biringen[16] reports success in transition control by periodic suction blowing. His approach is different from ours in that the wall forcing is applied at a single time step. This results in a reduction in the amplitude of the TS wave by a factor of 50% in one time step. To the extent that these results are not sensitive to the choice of time step and that significant transients are not generated by the impulsive forcing, they suggest the possibility of TS wave stabilization. After the suction-blowing condition has been imposed, the residual wave continues to grow at about the same rate as before. The mechanism for this growth is not clear, however, since the shear stress terms are reduced to near zero by the forcing boundary condition and remain small thereafter.

Kleiser and Laurien[21,22] have also performed simulations similar to ours in which, in addition to flow modification by suction and blowing at the wall, they have employed mass forcing and direct manipulation of the Fourier modes. They found that out-of-phase forcing is successful in damping out two-dimensional unstable modes in the linear range. In extending their results to three dimensions, they find that if the two-dimensional modes exceed a critical amplitude (usually about 1% of the peak mean velocity), they become extremely unstable to three-dimensional disturbances. Thus, Kleiser and Laurien have been unable to stabilize the flow with two-dimensional forcing once the amplitudes of the three-dimensional modes become on the order of the two-dimensional modes. While this is somewhat discouraging, the nature of three-dimensional wall motion interacting with these more complex flows has not yet been fully explored.

It is of interest to contrast the behavior of the energy fluxes in active wall stabilization with those for a compliant membrane. Work of Landahl[17] and Kaplan[23] has shown that for Blasius boundary-layer flow in the presence of a compliant membrane, modest increases in the critical Reynolds number are possible. Work in progress (in collaboration with J. Domaradzki) using a membrane model similar to that of Landahl and Kaplan has shown that, in coupled fluid-membrane systems, stabilization is associated with positive Reynolds stress production and negative pressure work terms, the opposite of active wall forcing. Thus, although the propagating wave continues to extract energy from the mean flow, there is a significant transfer of this energy to the membrane, where it is dissipated. In this case, the crest of the wall wave leads the high-pressure region of the fluid so that the fluid is doing work on the wall. There is presently active research addressing the question of whether more complex solid models, such as those producing an anisotropic response,[24] could significantly enhance flow stabilization.

Acknowledgments

This work was supported by the U.S. Office of Naval Research under Contract N00014-81-C-0454. The authors have benefitted from discussions with Drs. M.M. Reischman, J.A. Domaradzki, and F. Wan.

References

[1] Kramer, M.O., "Boundary Layer Stabilization by Distributed Damping," *Journal of American Society of Naval Engineers*, Vol. 72, 1960, p. 25 (also *Journal of Aeronautics and Space Sciences*, Vol. 27, 1960, p. 68).

[2] Bushnell, D.M., Hefner, J.N., and Ash, R.L., "Effect of Compliant Wall Motion on Turbulent Boundary Layers," *The Physics of Fluids*, Vol. 20, No. 10, Pt. II, 1977.

[3] McMichael, J.M., Klebanoff, P.S., and Mease, N.E., "Experimental Investigation of Drag on a Compliant Surface," *AIAA Progress in Astronautics and Aeronautics: Viscous Flow Drag Reduction*, Vol. 72, edited by G.R. Hough, AIAA, New York, 1980, p. 410.

[4] Hansen, R.J., Hunston, D.L., Ni, C.C., Reischman, M.M., and Hoyt, J.W., "Hydrodynamic Drag and Surface Deformations Generated by Liquid Flows over Flexible Surfaces," *AIAA Progress in Astronautics and Aeronautics: Viscous Flow Drag Reduction*, Vol. 72 edited by G.R. Hough, AIAA, New York, 1980, p. 439.

[5] Milling, R.W., "Tollmien-Schlichting Wave Cancellation," *Physics of Fluids*, Vol. 24, No. 5, 1981, pp. 979-98.

[6] McMurray, J.T., Metcalfe, R.W., and Riley, J.J., "Direct Numerical Simulations of Active Stabilization of Boundary Layer Flows," *Eighth Biennial Symposium on Turbulence, Proceedings of the Conference*, University of Missouri-Rolla, 1983, pp. 36-1–36-4.

[7] Liepmann, H.W., Brown, G.L., and Nosenchuck, D.M., "Control of Laminar Instability Waves Using a New Technique," *Journal of Fluid Mechanics*, Vol. 118, 1982, pp. 187-200.

[8] Liepmann, H.W. and Nosenchuck, D.M., "Active Control of Laminar-Turbulent Transition," *Journal of Fluid Mechanics*, Vol. 118, 1983, p. 201.

[9] Kuhn, G.D., Moin, P., Kim, J., and Ferziger, J., "Turbulent Flow in a Channel with a Wall with Progressive Waves," Paper presented at Symposium on Laminar/Turbulent Boundary Layers, New Orleans, Feb. 1984.

[10] Voigt, R.G., Gottlieb, D., and Hussaini, M.Y., *Spectral Methods for Partial Differential Equations*, SIAM, Philadelphia, 1984.

[11] Grosch, C.E. and Orszag, S.A., "Numerical Solution of Problems in Unbounded Regions: Coordinate Transforms," *Journal of Computational Physics*, Vol. 25, 1984, pp. 273-296.

[12] Orszag, S.A. and Kells, L.C., "Transition to Turbulence in Plane Poiseuille and Plane Couette Flow," *Journal of Fluid Mechanics*, Vol. 96, 1980, pp. 159-205.

[13] Orszag, S.A. and Patera, A.T., "Finite-Amplitude Stability of Axisymmetric Pipe Flow," *Journal of Fluid Mechanics*, Vol. 112, 1981, pp. 467-474.

[14] Monin, A.S. and Yaglom, A.M., *Statistical Fluid Mechanics: Mechanics of Turbulence*, Vol. 1, edited by J.L. Lumley, MIT Press, Cambridge, MA, 1971.

[15] Schlichting, H., *Boundary Layer Theory*, Pergamon Press, New York, 1955.

[16] Biringen, S., "Active Control of Transition by Periodic Suction-Blowing," *Physics of Fluids*, Vol. 27, No. 6, 1984, p. 1345.

[17] Landahl, M.T., "On the Stability of a Laminar Incompressible Boundary Layer Over a Flexible Surface," *Journal of Fluid Mechanics*, Vol. 13, 1962, p. 609.

[18] Benjamin, T.B., "Effects of a Flexible Boundary on Hydrodynamic Stability," *Journal of Fluid Mechanics*, Vol. 9, 1970, p. 513.

[19] Gad-el-Hak, M., Davis, S.H., McMurray, J.T., and Orszag, S.A., "On the Stability of the Decelerating Laminar Boundary Layer," *Journal of Fluid Mechanics*, Vol. 138, 1983, pp. 297-323.

[20] Klebanoff, P.S., Tidstrom, K.D., and Sargent, L.M., "The Three-Dimensional Nature of Boundary Layer Instability," *Journal of Fluid Mechanics*, Vol. 12, 1962, p. 1.

[21] Kleiser, L. and Laurien, E., "Three-Dimensional Numerical Simulation of Laminar-Turbulent Transition and Its Control by Periodic Disturbances," *Proceedings of the IUTAM Symposium on Laminar-Turbulent Transition/Novosibirsk*, Springer-Verlag, Berlin, 1985, pp. 29-37.

[22] Kleiser, L. and Laurien, E., "Numerical Investigation of Interactive Transition Control," AIAA Paper 85-0566, 1985.

[23] Kaplan, R.E., "The Stability of Laminar Incompressible Boundary Layers in the Presence of Compliant Boundaries," Sc.D. Thesis, Massachusetts Institute of Technology, Cambridge, 1964.

[24] Carpenter, P.W., "The Hydrodynamic Stability of Flows over Non-Isotropic Compliant Surfaces," Paper presented at APS 37th Annual Meeting, Division of Fluid Dynamics, Providence, RI, 1984.